Gamma-radiation effects in pure-silica-core photonic crystal fiber*

Wei Cai(蔡伟)[1,†], Ningfang Song(宋凝芳)[1], Jing Jin(金靖)[1], Jingming Song(宋镜明)[1], Wei Li(李伟)[2], Wenyong Luo(罗文勇)[2], and Xiaobin Xu(徐小斌)[1]

[1] *School of Instrument Science and Opto-electronic Engineering, Beihang University, Beijing* 100191, *China*
[2] *FiberHome Telecommunication Technologies CO., Ltd., Wuhan* 430000, *China*

(Received 29 April 2017; revised manuscript received 11 June 2017; published online 29 September 2017)

We investigated the steady state gamma-ray radiation response of pure-silica-core photonic crystal fibers (PSC-PCFs) under an accumulated dose of 500 Gy and a dose rate of 2.38 Gy/min. The radiation-induced attenuation (RIA) spectra in the near-infrared region from 800 nm to 1700 nm were obtained. We find that the RIA at 1550 nm is related with hydroxyl (OH^-) absorption defects in addition to the identified self-trapped hole (STH) defects. Moreover, it is proposed and demonstrated that reduced OH^- absorption defects can decrease the RIA at 1550 nm. The RIA at 1550 nm has effectively declined from 27.7 dB/km to 3.0 dB/km through fabrication improvement. Preliminary explanations based on the unique fabrication processes were given to interpret the RIA characteristics of PSC-PCFs. The results show that the PSC-PCFs, which offer great advantages over conventional fibers, are promising and applicable to fiber sensors in harsh environments.

Keywords: photonic crystal fibers, radiation-induced attenuation, color centers, fiber optics sensors

PACS: 42.81.Pa, 42.88.+h, 61.72.jn **DOI:** 10.1088/1674-1056/26/11/114211

1. Introduction

Photonic crystal fibers (PCFs) offer several distinct advantages compared with the conventional fibers and have been widely used in fiber sensors.[1–3] Two different types of PCFs are commercialized: solid-core PCF and air-core PCF. The application of air-core PCFs is still limited by the reliability, the splicing with other fibers, high costs, and high transmission loss.[4,5] Compared to air-core PCFs, solid-core PCFs are easier to handle and exhibit lower attenuation.[6] Furthermore, most solid-core PCFs are made with pure silica, which is known to be radiation-hardened under gamma-ray radiation. Thus, the pure-silica-core photonic crystal fibers (PSC-PCFs) are possible candidates for sensors in radioactive environments, such as the spaceborne fiber optic gyroscope. However, previous research on the steady-state gamma-ray radiation responses of PSC-PCFs showed complex results. Girard *et al.* found that the radiation induced attenuation (RIA) at 1550 nm of PSC-PCF is much higher than that of the conventional pure-silica-core fiber with fluorine-doped cladding.[7] Kosolapov *et al.* found that the RIA of PSC-PCF is very close to that of pure-silica-core fiber from 400 nm to 900 nm.[8,9] In an earlier study, we found that the PSC-PCF shows significantly higher RIA at 1310 nm and its recovery is slower than that of germanium-doped single mode fiber.[10] Theoretically, the PSC-PCF should be radiation-hardened. However, the practical high RIA makes it unsuitable for harsh environments. The steady-state gamma-ray radiation responses in the near-infrared part of the spectrum, which covers the common operating wavelength in communication and fiber sensors, should be further studied and decreased.

In this paper, we focus on the near-infrared region in the RIA spectrum of PSC-PCF after a steady state gamma-ray radiation with a total dose of 500 Gy and a dose rate of 2.38 Gy/min. We decomposed the RIA spectrum based on the Gaussian model and the defects that have been identified in the literature. It is found that the RIA at 1550 nm is related with not only the identified self-trapped hole (STH) defects but also hydroxyl (OH^-) absorption defects. After that, we proposed fabrication improvement to reduce the RIA at 1550 nm based on the reduction of OH^- absorption defects. The RIA at 1550 nm is decreased effectively from 27.7 dB/km to 3.0 dB/km. The experiment results demonstrate the contributions of OH^- absorption defects to RIA. Preliminary explanations based on the unique fabrication technology are given to interpret the RIA characteristics of the PSC-PCF samples. The results show that the PSC-PCFs are promising for fiber sensors in harsh environments.

2. Experiment

2.1. Tested optical fibers

The tested fiber samples were fabricated using the stack-and-draw process by FiberHome Telecommunication Technologies CO., Ltd. Figure 1 shows the typical spectral attenuation of PSC-PCF with a cross section photograph as an inset. All the fiber samples have similar geometry with a pitch of 5.6 μm, an enlarged hole diameter of 5.7 μm, and a small

*Project supported by the National Natural Science Foundation of China (Grant Nos. 61575012 and 61575013) and the National Key Scientific Instrument and Equipment Development Project, China (Grant No. 2013YQ040877).

†Corresponding author. E-mail: sdfz174caiwei@126.com

© 2017 Chinese Physical Society and IOP Publishing Ltd

hole diameter of 3.0 μm. The differences of the structural parameters between the PSC-PCF samples are within 3%. Similar microstructure, loss and spectral dependence levels were observed for the PSC-PCF samples. The details of the tested PSC-PCF samples are listed in Table 1. Each fiber sample is up to 200 m in length. The material of the fiber core and cladding is Heraeus F300 high purity fused silica tubes. The attenuations at 1550 nm of the samples are all below 4 dB/km. The samples mainly differ by the etching and dehydration process in their fabrication. Sample-1 and Sample-2 are two successive samples from the same original preform. They were made with the same material and the same fabrication processes. The preform bundle of Sample-3 was treated with an improved etching process before fiber drawing. The preform bundles of Sample-4 and Sample-5 were treated with improved etching and dehydration processes.

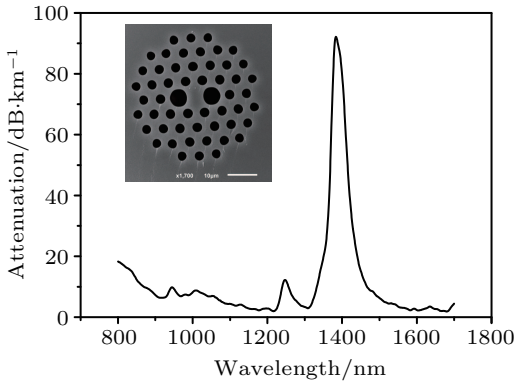


Fig. 1. Measured spectral attenuation of PSC-PCF.

Table 1. Tested PSC-PCF samples.

Sample ID	Length/m	Attenuation @1550 nm/dB·km^{-1}	Improved process
1	200	3.7	none
2	200	3.7	none
3	200	2.4	etching
4	200	2.0	etching and dehydration
5	200	1.8	etching and dehydration

2.2. Experiment setup

The experiment setup for measuring the RIA spectrum is shown in Fig. 2. A similar system has been reported in Ref. [11]. A supercontinuum white light source (NKT Photonics SuperK compact) with a spectrum from 500 nm to 2400 nm was used. Its output signal was split into eight paths by light splitting components. Four were used as references to compensate the variation of light intensity, and the others were guided into the samples under test. Only the tested samples were exposed to the ^{60}Co source and the other parts of our setup are kept in a shielded room outside the radiation room to avoid the influence of irradiation. Spectral attenuations in the near-infrared range (800 nm–1700 nm), both before and after irradiation, were measured using an optical spectral analyzer (OSA, Agilent 86142B). The RIA spectrum can be obtained by using the following formula:

$$\mathrm{RIA}(\lambda) = L_{\mathrm{B}}(\lambda) - L_{\mathrm{A}}(\lambda), \tag{1}$$

where $\mathrm{RIA}(\lambda)$ represents the RIA spectrum, and $L_{\mathrm{B}}(\lambda)$ and $L_{\mathrm{A}}(\lambda)$ (dB/km) represent the spectral attenuation measured before and after the fibers were irradiated, respectively.

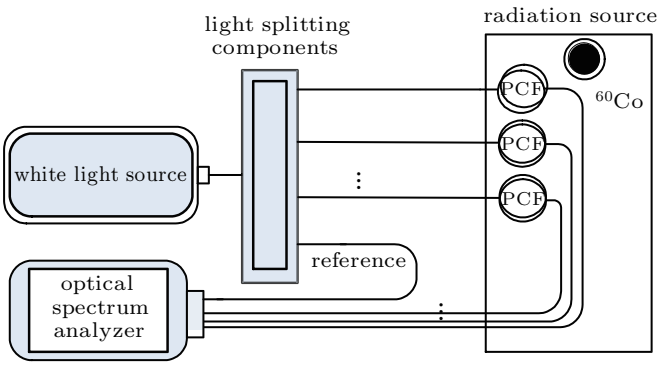


Fig. 2. (color online) Schematic of the experimental setup.

2.3. Experiment procedure

Two experiments were conducted to investigate the radiation characteristics of the PSC-PCFs. In the first experiment, we irradiated Sample-1 using a ^{60}Co gamma radiation source with a cumulative dose of about 500 Gy and a dose rate of 2.38 Gy/min at room temperature. After irradiation, the tested PSC-PCF sample was annealed at room temperature for a few days until most of the unstable defects were annealed and transformed. Then, we obtained the RIA spectrum of Sample-1. We observed that the RIA spectrum is related with OH^- absorption defects to some extent. It is expected that reduced OH^- absorption defects could lessen the RIA at 1550 nm. Thus, Sample-3, Sample-4, and Sample-5 were fabricated with different improved processes to remove the residual OH^- groups and contaminations in preform bundles. The details are illustrated in Table 1. To verify our extrapolation and investigate the influence of fabrication processes on the radiation responses of PSC-PCF samples, we irradiated the rest samples in Table 1 under the same conditions in the second experiment. Sample-2, which is derived from the same original preform as Sample-1 in the first experiment, acted as a comparison in the second experiment to ensure the reliability and repeatability of the experiment. After the same days annealing at room temperature, we obtained the RIA spectral responses of the rest samples.

3. Experiment results

3.1. Results of Sample-1

At the end of the first experiment, Sample-1 did not exhibit the anticipated lower RIA at 1550 nm than that of

the conventional germanium-doped fiber for its pure-silica core and cladding. For example, the RIA at 1550 nm of a germanium-doped fiber without phosphorus in the cladding reaches 4 dB/km.[7] However, Sample-1 showed a significantly high RIA of 28.1 dB/km at 1550 nm. Figure 3 shows the measured spectral attenuations of PSC-PCF Sample-1 before and after irradiation. The corresponding RIA spectrum obtained using Eq. (1) is shown in Fig. 4. We can see that the RIA around 1385 nm is much higher than that in the range of 1000 nm–1700 nm. The OH^- absorption defect, which is well known to produce an optical absorption (OA) band at about 1385 nm, is one of the main contributions to the total loss at 1550 nm in PCFs. Thus, we deduced that there must be a close relationship between the RIA at 1550 nm and the OH^- absorption defects.

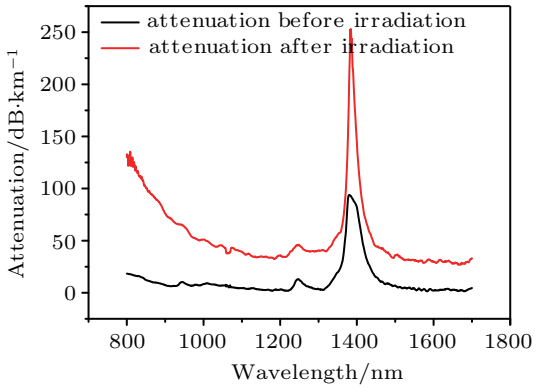


Fig. 3. (color online) Measured spectral attenuation of PSC-PCF Sample-1 before (black line) and after irradiation (red line).

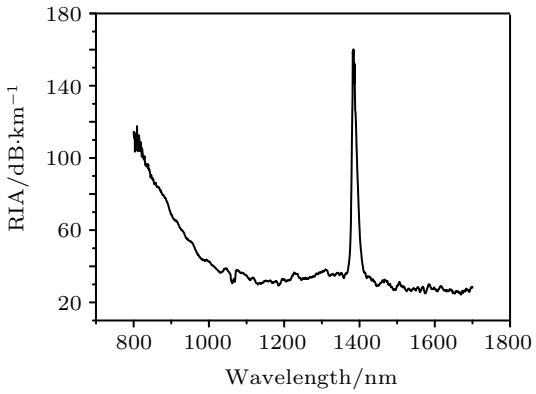


Fig. 4. RIA spectrum of PSC-PCF Sample-1.

In order to get more information on the defects in the fibers, we fitted the RIA spectrum with Gaussian functions, which are widely assumed for defects absorption in fibers.[12] The fitting formula is shown as

$$\mathrm{RIA} = \sum_{i=1}^{n} a_i \exp\left[-\left(\frac{E-E_i}{\omega_i}\right)^2\right], \tag{2}$$

$$E = h\frac{c}{\lambda}, \tag{3}$$

where E_i and ω_i represent the center and full width half maximum (FWHM) of the OA band of a defect, respectively; E represents the photon energy and a_i represents the absorption intensity of defects; n is the type of defect; the letters h, c, and λ denote the Planck constant, the velocity of light in the vacuum, and the operating wavelength, respectively.

The values of E_i and ω_i of the Si-related defects or color centers that have been identified in the literature[12] are listed in Table 2. The centers of OH^- defects' OA bands are 0.89 eV, 1.0 eV, and 1.3 eV, respectively. We extracted the contributions of OH^- defects by subtracting all the contributions of the defects displayed in Table 2 from the RIA spectrum. The fits of the pure-silica-core STHs (PSC-STHs), Si-related nonbridging oxygen hole center (Si-NBOHC), and OH^- defects contributions are quite raw. However, this allowed us to determine the main contribution to the RIA at 1550 nm.

Table 2. Main parameters of Si-related color centers in the literature.

Center name	E_i/eV	ω_i/eV
PSC-STH-1	2.6	1.12
PSC-STH-2	1.88	0.6
PSC-STH-3	0.7	0.3
PSC-STH-4	1.63	0.46
Si-NBOHC	1.97	0.2

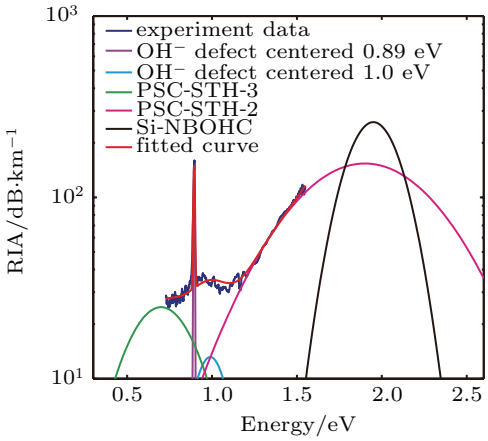


Fig. 5. (color online) Gaussian decomposition of the RIA spectrum of Sample-1 (blue line) with the Si-related defects from the literature and OH^- defects. The OA bands of different defects are shown as follows: PSC-STH-2 (pink line), PSC-STH-3 (green line), Si-NBOHC (black line), OH^- defect centered around 0.89 eV (purple line), and OH^- defect centered around 1.0 eV (cyan line). The contributions of other defects are negligible and not indicated.

The RIA spectrum of Sample-1 is decomposed into three parts including the STH defects, OH^- absorption defects, and Si-NBOHC as Fig. 5 shows. Only the OA bands of defects that have major contributions to the RIA spectrum are depicted. The contributions of other defects are negligible and not indicated in Fig. 5. The contributions of OH^- absorption defects take up $\sim 8\%$ of the whole RIA at 1550 nm according to the Gaussian model decomposition results. To minimize the contributions of OH^- absorption defects to the RIA at 1550 nm,

the fabrication process was improved. Then, we fabricated Sample-3, Sample-4, and Sample-5 using the improved etching and dehydration process for the second experiment.

3.2. Effects of the improved fabrication processes

The rest samples in Table 1 were irradiated in the second experiment under the same radiation dose and dose rate as the first experiment. The measured RIAs at 1550 nm of the rest PSC-PCF samples are shown in Table 3. We can see that improved processes effectively lower the RIA at 1550 nm from 27.7 dB/km to 3.0 dB/km. Sample-1 and Sample-2 showed the similar RIA spectrum at the end of the experiment, which demonstrates that the experiment conditions in the first and second experiments were almost the same.

Table 3. Measured RIA of the PSC-PCF samples.

Sample ID	Attenuation@1550 nm before radiation/dB·km^{-1}	RIA@1550 nm/dB·km^{-1}
2	3.7	27.7
3	2.4	5.9
4	2.0	4.8
5	1.8	3.0

Figure 6 shows the measured spectral attenuations of PSC-PCF Sample-5 before and after irradiation. The corresponding RIA spectrum obtained using Eq. (1) is shown in Fig. 7. We can see that the RIA around 1385 nm is almost the same as that in the range of 1200 nm–1700 nm after improving fabrication processes.

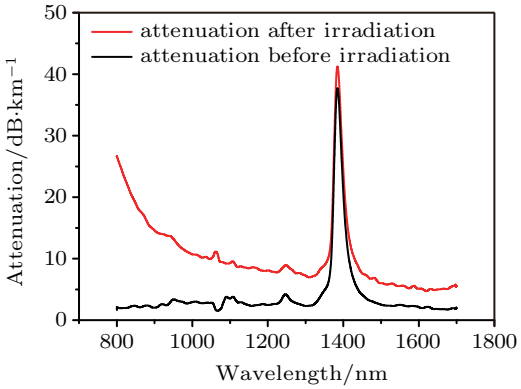


Fig. 6. (color online) Measured spectral attenuation of PSC-PCF Sample-5 before (black line) and after irradiation (red line).

The Gaussian decomposition result of Sample-5 is shown in Fig. 8. We can see that the absorption intensity of OH^- absorption defects and STH defects decline drastically compared with that of Sample-1. On the other hand, the absorption intensity of Si-NBOHC is almost the same as that of Sample-1.

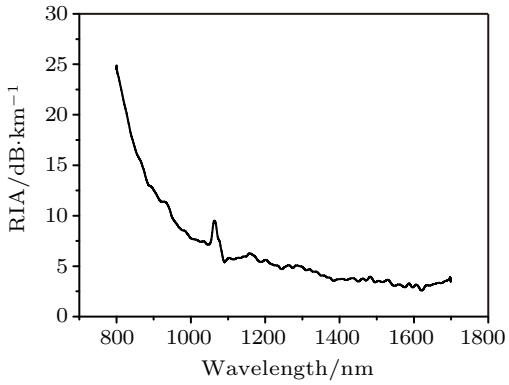


Fig. 7. RIA spectrum of PSC-PCF Sample-5.

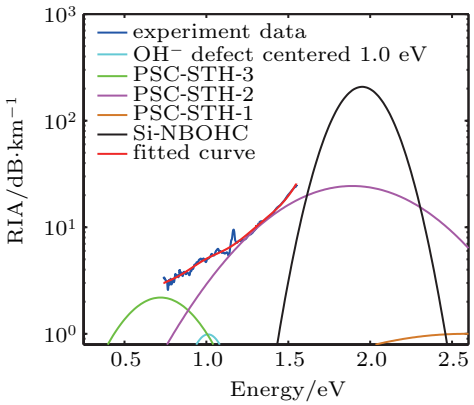


Fig. 8. (color online) Gaussian decomposition of the RIA spectrum of Sample-5 (blue line) with the Si-related defects from the literature and OH^- defects. The OA bands of different defects are shown as follows: PSC-STH-1 (brown line), PSC-STH-2 (pink line), PSC-STH-3 (green line), Si-NBOHC (black line), and OH^- defect centered around 1.0 eV (cyan line). The contributions of other defects are negligible and not indicated.

The RIA spectra of all the four PSC-PCF samples are decomposed using the same method mentioned above. The color center decomposition results are displayed in Table 4. As we can see from Table 4, the STHs play a dominant role in the RIA at 1550 nm. The Si-NBOHC seems to not contribute to the RIA at 1550 nm. The RIA and the contribution of OH^- absorption defects are decreased evidently from Sample-2 to Sample-3 by introducing the improved etching process. The total contribution of OH^- absorption defects to the RIA at 1550 nm is at least 2 orders of magnitude smaller than that of STH defects after improving fabrication processes.

Table 4. Decomposition of the RIA@1550 nm.

Sample ID	RIA@1550 nm/dB·km^{-1}	PSC-STHs	Si-NBOHC	OH^- defects
2	27.7	91.3%	0.0%	7.9%
3	5.9	98.8%	0.0%	0.5%
4	4.8	97.0%	0.0%	0.1%
5	3.0	95.1%	0.0%	0.0%

4. Discussion

The significantly higher RIA of Sample-1 in comparison with that of a germanium-doped fiber makes it unsuitable for

application in harsh environments. However, the high RIA can be reduced by improving fabrication processes from our results. Here, we present a preliminary explanation of the RIA characteristics in the experiments based on the unique stack-and-draw fabrication processes of the PSC-PCFs. In the fabrication, tens of capillaries and rods form large amounts of silica–air and silica–silica interfaces in preform bundles. Certain defect precursors could be generated at interfaces. Based on this assumption, two hypotheses were proposed to explain the RIA characteristics of PSC-PCFs.

4.1. Contribution of the STH defects to the RIA

The RIA of PSC-PCF at 1550 nm is mainly attributed to the STH absorption defects from our results. Chernov *et al.* showed that this kind of defect is stable at low temperature 77 K and unstable at 300 K. Moreover, this absorption was found to be strongly dependent upon the technology of the preform manufacturing and drawing conditions.[13] Kyoto *et al.* and Henschel *et al.* interpreted the STH color centers as a change in vibration modes as a result of gamma-ray radiation induced structural defects, which is long-lived.[14,15] Considering the fiber samples in Ref. [13] is only 4 m in length, the fact that we still observe STH defects at room temperature (about 300 K) is probably owing to our high sensitivity by using fiber samples of 200 m in length. From our experiment results, the RIA at 1550 nm drops drastically from 27.7 dB/km to 3.0 dB/km after fabrication improvement. The contributions of OH^- absorption defects take up about 8% (about 2.2 dB/km) of the whole RIA at 1550 nm in Sample-2. Most of the RIA reduction results from the decrease of the absorption intensity of STH defects. Thus, the absorption intensity of STH defects is related with fabrication processes, especially the treatment to the raw material, which is consistent with the results in Ref. [13]. Yamaguchi *et al.* showed that the STH defects are related to the effect of structural disorder.[16] Structural disorder could be induced at interfaces due to the large surface tension during the drawing process. Such STH defects may result from not only special fiber materials but also the interfaces between core and cladding. Many more silica–air and silica–silica interfaces exist in the unique stack-and-draw fabrication processes of PSC-PCFs, which may yield a higher degree of structural disorder or more defect precursors than that of conventional fibers. Thus, the STHs play a dominant role in the RIA of PSC-PCFs at 1550 nm. The density of STHs is also related with the fictive temperature of glass.[16,17] It seems possible to further decrease its contribution by optimizing the drawing parameters. In the next stage, we will investigate such drawing parameters in order to further reduce the PSC-PCF radiation sensitivity.

4.2. Contribution of the OH^- defects to the RIA

As is shown in Fig. 4, RIAs of Sample-1 near the OH^- absorption peaks (1240 nm and 1385 nm) are higher than those of other wavelengths in the investigated range, which indicates the existence of OH^- absorption defects. From the Gaussian decomposition results in Table 4, $\sim 8\%$ of the whole RIA at 1550 nm in Sample-2 can be attributed to the OH^- absorption defects. After the improvement of fabrication processes, the contribution of OH^- absorption defects in other samples is negligible. The initial material Heraeus F300 tube is specified with OH^- content below 1 ppm, with a typical value of 0.2 ppm. However, the fabrication of PCFs involves stacking of rods and capillaries, providing many opportunities for introducing small scratches and contaminations such as water vapor or dust particles on the inner and outer surfaces of the preform bundles. The high OH^- absorption defects of Sample-2 may come from the diffusion of OH^- into the glass. Since the diffusion constant follows an Arrhenius relationship with temperature, this form of contamination is particularly critical during the drawing process when the temperature is high.[18] The impurities and contaminations introduced in fabrication could induce some near-infrared and visible absorption bands after irradiation,[7] which affects the RIA at 1550 nm. The impurity contents in preform bundles are decreased after fabrication improvement, especially after the preform was treated with the improved etching process, and therefore the contributions of OH^- defects to the RIA at 1550 nm drop observably in other samples. It is likely that lower RIA levels can be reached by further eliminating contaminations.

5. Conclusion

We have investigated the steady state gamma-radiation responses of PSC-PCFs in the near-infrared wavelength. The results reveal the dominant role of STH defects in the RIA at 1550 nm. Moreover, we found that OH^- absorption defects have contributions to the RIA spectrum. The contribution of OH^- absorption defects to RIA at 1550 nm is negligible after fabrication improvement and the RIA at 1550 nm has declined evidently from 27.7 dB/km to 3.0 dB/km. The level of radiation resistance achieved is superior to most commercial Ge-doped single-mode fibers[7,19,20] and conventional PSC fibers[11] at 1550 nm under similar conditions, to the best of our knowledge. Our study provides an explanation of the RIA characteristic of PSC-PCFs based on the unique stack and draw fabrication process, which produces STH absorption defects and the OH^- absorption defects. The generation efficiency of defects is also affected by other parameters of the material, fictive temperature for example. It is possible to further decrease their contributions and consequently to fabricate more radiation-hardened PSC-PCFs. Considering the remarkable properties of PSC-PCFs such as low bending loss, design

flexibility, and high birefringence with a lower sensitivity to temperature, they are good candidates for future fiber sensors in harsh environments.

Acknowledgment

The work was performed at the Beihang University and FiberHome Telecommunication Technologies CO., Ltd. The authors would like to acknowledge all the staff in the FiberHome Telecommunication Technologies CO., Ltd. for their technical feedback and support in the PCF fabrication.

References

[1] Knight J C 2003 *Nature* **424** 847
[2] Hoo Y L, Jin W, Shi C Z, Ho H L, Wang D N and Ruan S C 2003 *Appl. Opt.* **42** 3509
[3] Qin W, Li S G, Xue J R, Xin X J and Zhang L 2013 *Chin. Phys. B* **22** 074213
[4] Lefèvre H 2014 *Fiber Optic Gyroscope* (2nd Edn.) (Artech House) pp. 328–329
[5] Rizzolo S, Boukenter A, Allanche T, Perisse J, Bouwmans G, Hamzaoui H El, Bigot L, Ouerdane Y, Cannas M, Bouazaoui M, Mace J R, Bauer S and Girard S 2016 *IEEE Trans. Nucl. Sci.* **63** 2038
[6] Tajima K, Zhou J, Nakajima K and Sato K 2004 *J. Lightwave Technol.* **22** 7
[7] Girard S, Yahya A, Boukenter A, Ouerdane Y, Meunier J P, Kristiansen R E and Vienne G 2002 *IEEE Electron. Lett.* **38** 1169
[8] Kosolapov A F, Semjonov S L and Tomashuk A L 2006 *Proceedings of SPIE* (Vol. 6193) *Reliability of Optical Fiber Components, Devices, Systems, and Networks III* p. 6193E
[9] Kosolapov A F, Nikolin I V, Tomashuk A L, Semjonov S L and Zabezhailov M O 2004 *Inorg. Mater.* **40** 1229
[10] Wang X Q, Zhang C X, Jin J, Song N F and Xu H J 2011 *Optik* **122** 1918
[11] Jin J, Li Y, Zhang Z C, Wu C X and Song N F 2016 *Chin. Phys. B* **25** 084213
[12] Girard S, Ouerdane Y, Bouazaoui M, Marcandella C, Boukenter A, Bigot L and Kudlinski A 2011 *Opt. Express* **19** 21760
[13] Chernov P V, Dianov E M, Karpechev V N, Kornienko L S, Rybaltovskll A O, Sokolov V O and Sulimov V B 1989 *Phys. Stat. Sol. B* **156** 663
[14] Kyoto M, Chigusa Y, Watanabe M O O E M, Matsubara T, Yamamoto T and Okamoto S 1989 *J. Nucl. Sci. Technol.* **26** 507
[15] Henschel H, Köhn O and Schmidt H U 1996 *Proceedings of SPIE* (Vol. 2811) *Photonics for Space Environments IV* p. 68
[16] Yamaguchi M, Saito K and Ikushima A J 2003 *Phys. Rev. B* **68** 153204
[17] Alessi A, Girard S, Cannas M, Agnello S, Boukenter A and Ouerdane Y 2012 *J. Lightwave Technol.* **30** 1726
[18] Frosz M H, Ahmed G, Lapshina N, Keding R, Babic F, Joly N Y and Philips R 2016 *Opt. Mater. Express* **6** 2975
[19] Wen J X, Peng G D, Luo W Y, Xiao Z Y, Chen Z Y and Wang T Y 2011 *Opt. Express* **19** 23271
[20] Olantera L, Sigaud C, Troska J, Vasey F, Petrovich M N, Poletti F, Wheeler N V, Wooler J P and Richardson D J 2013 *J. Instrum.* **8** C12010